Electron motion induced by magnetic pulse in a bilayer quantum wire

T. Chwiej*

AGH University of Science and Technology, al. A. Mickiewicza 30, 30-059 Cracow, Poland

(Received 18 January 2016; revised manuscript received 4 May 2016; published 3 June 2016)

We consider theoretical stimulation of electron motion in a quantum wire by means of ultrashort magnetic pulses of time duration between several and a few tens of picoseconds. In our considerations, an electron is confined in a nanowire which consists of two vertically stacked tunnel-coupled layers. If a magnetic pulse pierces this nanowire and its direction is parallel to the plane established by the layers, and additionally, it is perpendicular to the wire's axis, then the eigenstates of a single electron energy operator for vertical direction are hybridized by the off-diagonal terms of the full Hamiltonian. These terms depend linearly on the momentum operator, which means that such magnetically forced hybridization may induce electron motion in a nanowire. The classical counterpart of this quantum-mechanical picture is a situation in which the rotational electric field generated by a time-varying magnetic field pushes the charge densities localized in the upper and lower layers in opposite directions. We have found, however, that for an asymmetric vertical confinement in a bilayer nanowire, the major part of the single electron density starts to move in the direction of the local electric field in its layer forcing the minority part to move in this direction as well. It results in coherent motion of both densities in a particular direction. We analyze the dynamics of such motion in dependence on the time characteristics of a magnetic pulse and discuss potential applications of this effect in the construction of a magnetic valve.

DOI: 10.1103/PhysRevB.93.235405

I. INTRODUCTION

The tunnel coupling between two quantum wires has a large impact on single electron transport properties [1–5]. This kind of coupling is very sensitive to an external magnetic field which can modify its strength or even completely destroy it. The scale of magnetic field influence on tunnel coupling depends on the magnetic field strength and on mutual arrangement of the wire's axis and the magnetic field's direction [6,7]. If the magnetic field is parallel to the wire's axis, it squeezes the wave functions of the magnetosubbands within each layer which diminishes the interlayer tunneling [7,8]. On the other hand, if it is set perpendicularly to the wire's axis as well as to the layers, which are coupled laterally or vertically, it can hybridize the magnetosubbands originated in different layers. This modifies to a large extent the energy dispersion relation $E(k)$. In such case, the pseudogaps are opened in the energy spectrum and the negative energy dispersion relation appears [3,9]. As we have shown in our last paper, hybridization which leads to the formation of pseudogaps can be used for tuning the magnitude of spin polarization of the wire's conductance. This can be done provided that the wire has a low density of defects [10].

In the present paper we study the dynamics of electron motion that can be induced by magnetic pulse only. An electron is confined in a semiconductor nanowire which consists of two vertically stacked transport layers made of InGaAs or GaAs semiconductor materials. Magnetic acceleration or deceleration of an electron in such nanostructure can be conducted provided that (i) the wave functions originated from different layers are hybridized, and (ii) the time duration of the magnetic pulse is between several and a few tens of picoseconds. At present, such short magnetic pulses can be generated by the application of Auston's photoconductive switches [11,12] or by the off-resonant magnetization of ferromagnetic thin films with terahertz laser pulses [13]. When the magnetic pulse pierces a bilayer nanosystem and the direction of the temporary magnetic field is parallel to the layers as well as perpendicular to the transport direction, then the states corresponding to different excitations in the vertical direction are temporarily hybridized. The Hamiltonian's off-diagonal elements responsible for this coupling are linear with respect to the electron's momentum operator and consequently such hybridization must change its motion energy. In classical electrodynamics, this change of the particle's momentum stems from the charge density interaction with the rotational electric field generated by the time-varying magnetic field. Since this electric field is parallel and antiparallel to the nanowire's axis in the upper and lower layer, respectively, the upper and lower parts of single electron density are pushed in opposite directions (the action of a temporary rotational electric field on the electron wave packet confined in a vertical bilayer nanowire is schematically depicted in Fig. 1). If the electron density is evenly distributed between layers, e.g., for symmetric vertical confinement, then both upper and lower densities move along the wire in opposite directions thus giving no current. We show, however, that in a nanostructure with asymmetric vertical confinement, the major part of the electron density which has been confined in one layer and next was pushed by an electric field in a particular direction, may simultaneously drag the minority part in this direction against the electric field in the second layer. In such case, a magnetic pulse may effectively change an expectation value of the electron's position and generate nonzero current flow in a system. The dynamics of electron motion induced by a magnetic pulse depends on several factors such as, e.g., the time length of magnetic pulse, an electron effective mass, and on that, whether the magnetic field finally vanishes ($B = 0$ for $t > t_{\mathrm{imp}}$) or not ($B > 0$ for $t > t_{\mathrm{imp}}$) after the pulse is finished. In the latter case, which is an analog of switching the magnetic field on, the electron motion in a constant magnetic

*chwiej@fis.agh.edu.pl

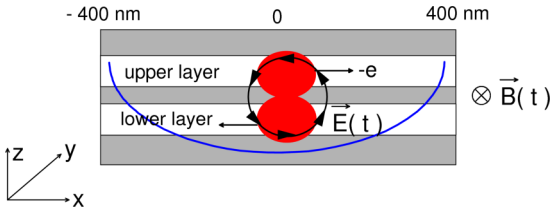

FIG. 1. The cross section of the model bilayer nanowire considered in this paper. The electron's motion in the x direction within a harmonic oscillator potential (blue line) is stimulated by a rotational electric field generated by the time-varying magnetic field which is directed along the y axis.

field is governed by the magnetic force which for longer times destroys the coherent motion of the upper and lower parts of the electron density.

The paper is organized as follows. In Sec. II we present a theoretical model based on the time-dependent Schrödinger equation expressed in mixed energy and space-position form which provides an essential quantum equation of motion. Example results of simulations of electron motion induced by a magnetic pulse in a bilayer wire are presented and discussed in Sec. III, while potential applications of this effect are shown at the end of this section. Finally, conclusions are given in Sec. IV.

II. THEORETICAL MODEL

We start our considerations with single electron Hamiltonian $\widehat{H} = (\widehat{\boldsymbol{p}} + e\boldsymbol{A})^2/2m^* + V_c(\boldsymbol{r})$. Throughout the paper we will use the time-dependent vector potential in nonsymmetric gauge $\boldsymbol{A}(t) = (zB(t),0,0)$ for which the magnetic field is parallel to the layers and perpendicular to the transport direction, namely, $\boldsymbol{B} = (0,B(t),0)$. We assume the electron can move along the wire in the x direction and may tunnel between two vertical layers which establish a double-well potential in the z direction. The electron motion in the y direction is frozen to the ground state and is neglected in further discussions. A sketch of the confining potential is shown in Fig. 1. In the considered model, the confining potential in the x and z directions is separable, i.e., $V_c(x,z) = V_1(x) + V_2(z)$. Therefore, the part of the Hamiltonian dependent on the z variable, that is, $\widehat{h}_z = -(\hbar^2/2m^*)\partial/\partial z^2 + V_2(z)$, can be diagonalized independently from the rest. Its lowest $M = 10$ eigenstates $f_k(z)$ have been used as basis functions in further considerations. The matrix elements of the full Hamiltonian calculated for this basis have the mixed energy and position-space form

$$\widehat{H}_{k,k'} = \left[\widehat{T}_x + V_1(x) + E_k^{(z)}\right]\delta_{k,k'} + \hbar\omega_c Z_{k,k'}^{(1)}\widehat{k}_x + \frac{m^*\omega_c^2}{2}Z_{k,k'}^{(2)}, \tag{1}$$

where $\widehat{T}_x$ is the kinetic operator for the x direction, $E_k^{(z)}$ is a kth eigenenergy of Hamiltonian $\widehat{h}_z$, $\omega_c = eB/m^*$ is the cyclotron frequency, matrix elements $Z_{k,k'}^{(1)}$ and $Z_{k,k'}^{(2)}$ are defined as $Z_{k,k'}^{(m)} = \langle f_k|z^m|f_{k'}\rangle$, and $\widehat{k}_x = \widehat{p}_x/\hbar = -i\partial/\partial x$. The Hamiltonian given in Eq. (1) depends on time through the second and third terms which include ω_c. For the single electron wave function defined as $\Psi(x,z,t) = \sum_{k=1}^{M}\psi_k(x,t)f_k(z) = \boldsymbol{\psi}(x,t)\cdot\boldsymbol{f}(z)$, its components $\psi_k(x,t)$ are solutions of the time-dependent Schrödinger equation

$$i\hbar\frac{\partial}{\partial t}\begin{bmatrix}\psi_1(x,t)\\ \psi_2(x,t)\\ \vdots\\ \psi_M(x,t)\end{bmatrix} = \begin{bmatrix}H_{11} & H_{12} & \dots & H_{1M}\\ H_{21} & H_{22} & & H_{2M}\\ \vdots & & \ddots & \vdots\\ H_{M1} & H_{M2} & \dots & H_{MM}\end{bmatrix} \times \begin{bmatrix}\psi_1(x,t)\\ \psi_2(x,t)\\ \vdots\\ \psi_M(x,t)\end{bmatrix}, \tag{2}$$

with matrix elements $H_{k,k'}$ defined in Eq. (1).

We define the confining potential within two coupled layers in the vertical direction with the following formula [5,14]:

$$V_2(z) = V_{\max}\{\sin[(1+z/b)\pi/2] + \alpha\sin[\pi(1+z/b)]\}. \tag{3}$$

The confining potential $V_2(z)$ is symmetric for $\alpha = 0$ while the upper layer becomes deeper than the lower one for $\alpha > 0$. The shape of $V_2(z)$ is crucial for the electron dynamics in a quantum wire. For $\alpha = 0$, the basis wave functions $f_k(z)$ have well defined parities. Then, the third term in Eq. (1) disappears and only the second term can mix components $\psi_k(x)$ and $\psi_{k'}(x)$ for $k \neq k'$ through the off-diagonal elements $H_{kk'}$ and $H_{k'k}$ in Eq. (2). On the other hand, when $\alpha > 0$, the third term in Eq. (1) also gives a contribution to the off-diagonal elements in Eq. (2) and to the diagonal ones as well. Thus, mixing of these components is essential for inducing an electron motion by means of the magnetic pulse. If mixing is absent during the time evolution, $\psi_k(x,t)$ components of the electron's wave function evolve independently according to the stationary solutions. Because hybridization of the vertical states takes place only for $B \neq 0$, the momentum of the electron can be effectively changed in two cases: (i) when the magnetic pulse temporarily pierces the nanowire ($\partial B/\partial t \neq 0$), or (ii) when the electron moves in the wire and it simultaneously interacts with the stationary magnetic field ($\partial B/\partial t = 0$ and $B \neq 0$). Both cases provide qualitatively different results and will be discussed in the next section.

Even though the last two terms in Eq. (1) can mix the wave functions $\psi_k(x)$ and $\psi_{k'}(x)$, only the second term may force an electron to change its position. The proof is straightforward if for a while, we take into consideration only two lowest basis states f_k and neglect the upper ones due to, as we will show further, their small contributions to wave function $\Psi(x,z,t)$. Then, the x-dependent part of the wave function for the ground state of electron for $B = 0$ and $t = 0$ is given by $\boldsymbol{\psi}(x,t) = (\psi_1(x,0),\psi_2(x,0)) = (g_0(x),0)$, where $g_0(x)$ is an arbitrarily chosen normalized square integrable function. If we now skip in Eq. (2) the term $\hbar\omega_c Z_{k,k'}^{(1)}\widehat{k}_x$ and replace the time derivative with the forward first-order finite difference formula, then in the first time step we get approximations for components of $\boldsymbol{\psi}(x,t)$: (i) $\psi_1(x,\Delta t) = (1 - i\Delta t m^*\omega_c^2 E_1/\hbar)\psi_1(x,0)$, where E_1 is the total energy of the electron at $t = 0$, and (ii) $\psi_2(x,\Delta t) = -(i\Delta t m^*\omega_c^2 Z_{21}^{(2)}/2)\psi_1(x,0)$. In other words, part of $g_0(x)$ is shifted from ψ_1 to ψ_2 and vice versa for further time steps but the shape of $|\boldsymbol{\psi}(x,t)|^2 = \langle\Psi|\delta(x-x')|\Psi\rangle$ will

remain unchanged. Simply, this term represents a diamagnetic shift which is responsible for optimization of the wave function's shape in the z direction, i.e., for its stronger localization in the magnetic field. The dynamics of the electron motion during the simulation is governed thus by the term $\hbar\omega_c Z^{(1)}_{k,k'}\widehat{k}_x$ which includes a derivative with respect to the x variable.

We have simulated an electron motion in a bilayer nanowire by finding solutions of time-dependent Schrödinger equation (2) in subsequent discrete time instants. For this purpose we used the fourth-order Runge-Kutta method and the time step was set to $\Delta t = 10^{-4}$ ps. The length of the quantum wire was limited to 800 nm and a smooth confining potential of quantum oscillator $V_1(x) = m^*\omega_0^2 x^2/2$ with oscillator strength $\hbar\omega_0 = 0.5$ meV was imposed along the wire's axis. This spatial constriction allows us to study the electron motion for quite long times after the magnetic pulse is finished. Such conduct is particularly important if an influence of magnetic force, appearing when $B_y = \text{const}$, on motions of the upper and lower parts of the electron wave packet is considered. The basis functions $\{f_k\}$ were also found numerically. For this purpose, Hamiltonian $\widehat{h}_z$ was first discretized on spatial mesh, and next was diagonalized providing its eigenstates $\{f_k\}$. In calculations we have used 200 and 400 nodes for meshes in the z and the x direction, respectively. All simulations were preceded by diagonalization of Hamiltonian (2) in order to prepare the starting wave packet $\Psi(x,z,t=0)$.

The value of parameter b, which defines the extent of the vertical confinement in Eq. (3), equals 30 nm [7,14]. The height of the tunnel barrier between the upper and lower layers depends on the magnitude of $V_{\max}$. Its value was set to 150 meV for which the energy splitting between the lowest bounding and antibounding basis states $\{f_k\}$ for symmetric vertical confinement ($\alpha = 0$) equals $E^{(z)}_{21} = E^{(z)}_2 - E^{(z)}_1 = 1.95$ meV for GaAs ($m^* = 0.067$) and $E^{(z)}_{21} = 9.8$ meV for InGaAs ($m^* = 0.04$). Note, that for $\alpha > 0$ the value of $\Delta E^{(z)}_{21}$ grows which in turn limits the mixing of ψ_k and $\psi_{k'}$ components. This cannot be avoided, however, because for $\alpha = 0$ both parts of the electron wave packet localized in the upper and lower layers move in opposite directions (see Fig. 1).

III. RESULTS

A. Stimulation of electron motion by single magnetic pulse

We start the presentation of our results with a case in which an electron is accelerated by a single magnetic pulse. The following expression defines the pulse's shape:

$$B(t) = B_m \sin(\pi t/t_{\text{imp}})\Theta(t)\Theta(t_{\text{imp}} - t), \tag{4}$$

where $\Theta(t)$ is the Heaviside step function. In calculations we have set the amplitude of the magnetic field equal to $B_m = 5$ T, while the time duration of the magnetic pulse was changed within the range $t_{\text{imp}} = 5$–50 ps.

Figure 2 shows the modulus of contributions of four basis states (out of ten) f_k to the wave function $\Psi(x,z,t)$ for the magnetic pulse of time duration $t_{\text{imp}} = 10$ ps. These contributions were calculated according to formula $|c_k(t)| = \sqrt{\langle\psi_k(x,z,t)|\psi_k(x,z,t)\rangle}$. In Fig. 2 we see that the main contributions to $\Psi(x,z,t)$ deliver f_1 and f_2 states, while

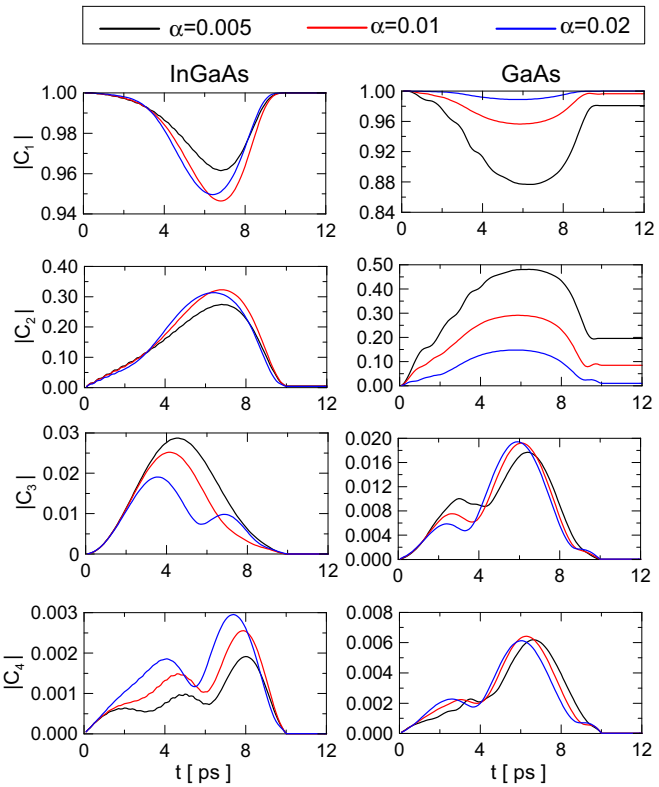

FIG. 2. Contributions of the first four (out of ten) basis functions $\{f_k\}$ to $\Psi(x,z,t)$ for time duration of magnetic pulse $t_{\text{imp}} = 10$ ps and three values of asymmetry factor $\alpha = 0.005, 0.01, 0.02$.

contributions from f_3 and f_4 are one and two orders of magnitude times smaller than that for f_2. This generally holds for all α values for the InGaAs and GaAs nanowires. For this reason, in simulations we have limited the number of these basis functions to $M = 10$, which is enough to ensure the convergence of the results. Due to the small effective mass of the electron in a InGaAs nanowire ($m^* = 0.04$) resulting in wider energy splitting of the lowest bounding and antibounding states (E^z_{21}), mixing of the two lowest vertical eigenstates is significantly less effective than for a GaAs nanowire. Moreover, for a InGaAs nanowire, contributions from states with indices $k \geqslant 3$ always vanish after the pulse is finished, while as we see in the second row in Fig. 2, an electron can still partly occupy the first excited state ($k = 2$). It means that in the InGaAs wire, the energy gained by an electron is almost completely converted into motion energy, while in the second case (the GaAs wire), besides the increase in the electron's motion energy it can also be excited in the vertical direction.

In Fig. 3(a) we present the time variations of the electron's position in the upper and lower layers obtained according to Eqs. (6) and (7) (see description below) for a symmetric bilayer nanowire ($\alpha = 0$) made of InGaAs. The magnetic pulse starts at $t = 0$ and ends at $t = 20$ ps. Within this time interval, two parts of the electron wave packet localized in the upper and lower layers oscillate in the x direction but with opposite velocities, i.e., the upper part starts to move to the right while the second, localized in the lower layer, moves to the left. Then, both change directions of their motions three times due to reflections within the left and right barrier regions.

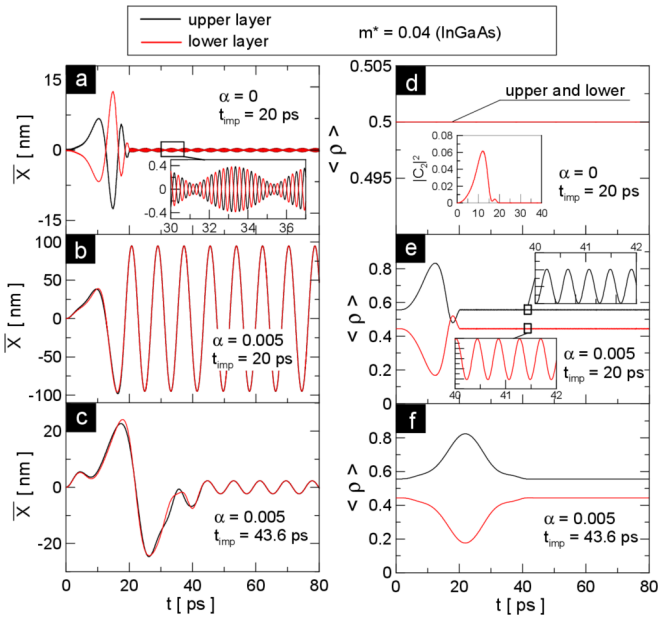

FIG. 3. Expectation value of the electron's position (left column) and amount of density (right column) localized in the upper (red color) and in the lower layer (black color) during the simulation for $\alpha = 0$ (first row) and $\alpha = 0.005$ (second and third rows). Insets in (a) and (e) show zooms of oscillations of $\bar{x}$ and $\langle\rho\rangle$ remaining after the magnetic pulse finally vanishes. The inset in (d) shows the value of occupation factor $|c_2|^2$ of the second vertical eigenstate. Calculations were performed for parameters $m^* = 0.04$ (InGaAs), $\Delta E^z_{21} = 9.8$ meV [(a),(d)] and $\Delta E^z_{21} = 9.9$ meV in (b)–(f).

This, in turn, generates oscillations of their positions in layers. After the magnetic field eventually vanishes, these oscillations are strongly dumped but do not disappear entirely. The inset in Fig. 3(a) shows that even for $t > t_{\rm imp}$ the amplitude of oscillations becomes very small and remains stable for longer times. The beating pattern shown in this inset appears due to an overlap of two kinds of oscillations. The first type of oscillations has the time period $T_1 = 8.3$ ps, while for the second it equals $T_2 = 0.44$ ps. To determine their origins we first calculated an expectation value of electron position in the upper layer according to formula $\langle x\rangle_{z>0} = \langle\Psi|x\Theta(z)|\Psi\rangle$. Exactly at the moment the magnetic pulse ends ($B = 0$), the electron wave function can be expressed as $\Psi(x,y,z,t_{\rm imp}) = \sum_k \psi_k(x,t_{\rm imp}) f_k(z) g_0(y)$. The x-dependent parts of the wave function can be then expressed as the linear combinations of Hermite polynomials, i.e., the eigenstates of quantum oscillator

$$\Psi(x,y,z,t) = \sum_k \sum_\mu d_{k,\mu}\phi_\mu(x) f_k(z) g_0(y) e^{-i(E^x_\mu + E^z_k + E^y_0)t/\hbar}. \tag{5}$$

In the above equation, $d_{k,\mu}$ are expansion coefficients found at $t = t_{\rm imp}$, $\phi_\mu(x) = C_\mu \mathcal{H}_\mu(x) e^{-x^2}$ are normalized Hermite polynomials, while the three arguments appearing in the phase factor are the eigenenergies for the quantized motion of the electron in the x (E^x_μ), y (E^y_0), and z (E^z_k) directions. According to this definition, the position of the electron in the upper layer [dependence on $g_0(y)$ and E^y_0 disappear after integration over the y variable] reads

$$\langle x\rangle_{z>0} = \sum_{k,m}\sum_{\mu,\nu} d^*_{k,\mu} d_{m,\nu} \langle\phi_\mu|x|\phi_\nu\rangle \langle f_k|\Theta(z)|f_m\rangle \times e^{i\Delta E^x_{\mu,\nu} t/\hbar} e^{i\Delta E^z_{k,m} t/\hbar}. \tag{6}$$

Because the probability densities confined in the layers may differ from unity, we have normalized an expectation value of the electron's position in the upper (or lower for $z < 0$) layer,

$$\bar{x}_{z>0} = \frac{\langle x\rangle_{z>0}}{\langle\Psi|\Psi\rangle_{z>0}}. \tag{7}$$

The matrix elements $\langle\phi_\mu|x|\phi_\nu\rangle$ appearing in Eq. (6) have nonzero values only if $\mu = \nu \pm 1$, that is, for $\Delta E_{\mu,\nu} = \pm\hbar\omega_0$. In such case, oscillations with longer period $T_1 = h/\Delta E_{\mu,\mu\pm1} = 8.3$ ps appear, provided that, ΔE^z_{km} vanishes for $k = m$ in Eq. (6). Otherwise, when conditions $k \neq m$ and $\mu = \nu \pm 1$ are fulfilled, the total phase factor oscillates with frequency depending on $\Delta E = \Delta E^z_{21} + \hbar\omega_0 = 10.33$ meV, which gives the period equal to $T_2 = 0.44$ ps. This indicates that even though the basis functions $\{f_k\}$ are decoupled due to $\omega_c = 0$ [see Eq. (1)], even a small admixture of the f_2 state in the wave function defined in Eq. (5) may force an electron to oscillate along the nanowire.

Equation (6) can be further utilized in calculations of $\langle\rho\rangle_{z>0}$ if the terms $\langle\phi_\mu|x|\phi_\nu\rangle$ are substituted by $\langle\phi_\mu|\phi_\nu\rangle = \delta_{\mu,\nu}$. This substitution eliminates the dependence of the total phase on $\Delta E^x_{\mu,\nu} = 0$ but leaves it still dependent on the $\Delta E^z_{k,m}$ value. However, if vertical confinement in the nanowire is symmetric [see the results for $\alpha = 0$ in Fig. 3(d)], oscillations in $\langle\rho\rangle_{z>0}$ are absent since the upward and downward density flows cancel each other. These are visible only for $\alpha = 0.005$ [Fig. 3(e)] but their amplitude is very small mainly due to the large energy splitting $\Delta E^{(z)}_{21}$ in the InGaAs nanowire.

For $\alpha > 0$, the confinement energy in the lower layer becomes higher than in the upper layer. Then, at the beginning of simulation, the larger part of the electron density is localized in the upper layer [see Figs. 3(e) and 3(f)]. Therefore, when the magnetic field starts to grow, the major part of the electron wave packet moves to the right but this time the rest of it is also pulled in this direction. In Figs. 3(b) and 3(c) we see that both densities move coherently and independently of the time duration of the magnetic pulse. Due to the asymmetry which has been introduced into the confining potential in the vertical direction, the amount of density in each layer is smoothly changed when $\partial B/\partial t \neq 0$ and $t < t_{\rm imp}$. For $t > t_{\rm imp}$ both become fixed [see Figs. 3(e) and 3(f)] besides the small oscillations with frequency $\omega'_2 = 2\pi/T'_2$ visible in the inset in Fig. 3(e). Their appearance means that some part of the energy delivered to the system by a magnetic pulse was used to excite an electron in the vertical direction. However, due to quite a difference in excitation energies for the longitudinal ($\hbar\omega = 0.5$ meV) and vertical directions ($\Delta E^{(z)}_{21} \geqslant 9.8$ meV for InGaAs), excitations of the electron along the nanowire's axis are preferable to those for the vertical direction.

We have repeated the calculations of $\bar{x}$ and $\langle\rho\rangle$ for a heavier effective mass. The results for a GaAs bilayer nanowire are shown in Fig. 4. Due to a few times lower energy splitting $\Delta E^{(z)}_{21}$ in the GaAs than in the InGaAs wire, oscillations in $\bar{x}$ for $\alpha = 0$ are more pronounced [Fig. 4(a)] but for the same

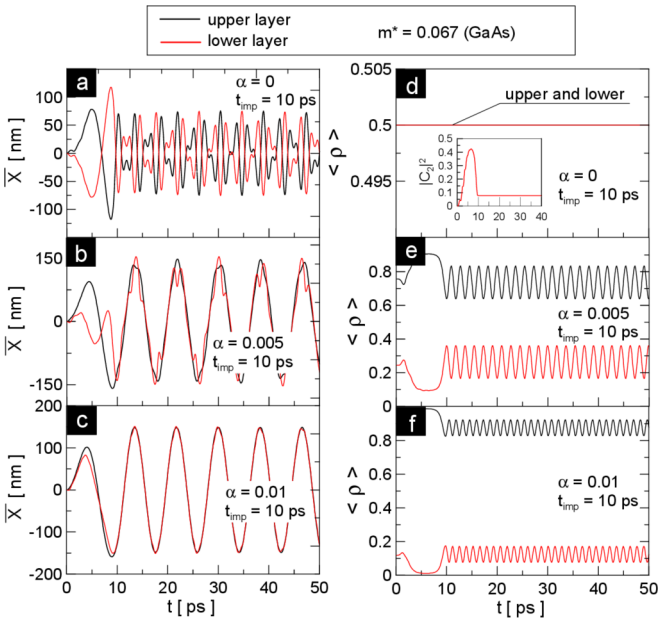

FIG. 4. The same as in Fig. 3 but for heavier effective mass $m^* = 0.067$. Energy splitting between the two lowest bounding and antibounding vertical eigenstates equals $\Delta E_{21}^z = 1.95$ meV in (a) and (d), $\Delta E_{21}^z = 2.28$ meV in (b) and (e), and $\Delta E_{21}^z = 3.06$ meV in (c) and (f).

reason as previously, i.e., due to symmetry constriction, the amount of density confined in the lower and upper layers is the same [see Fig. 4(d)]. For a slightly broken symmetry in the vertical confining potential ($\alpha = 0.005$), a major part of the density initially localizes in the upper layer. Due to a small value of $\Delta E_{21}^{(z)} = 2.28$ meV in GaAs in comparison to the longitudinal excitations ($\hbar\omega_0 = 1$ meV), the significant remnant of excitation of the f_2 state remains large after the magnetic pulse is finished. It results in a large amplitude of density oscillations in the vertical direction [see Fig. 4(e)]. Such interlayer periodic flow of density naturally perturbs an oscillatory character of electron motion along the wire's axis, albeit as we see in Fig. 4(b) motion of the major part of the density (black color) is less perturbed than that of the minority one (red color). For larger confinement asymmetry ($\alpha = 0.01$), the charge density oscillations in the vertical direction are smaller [Fig. 4(f)] because of the larger value of $\Delta E_{21}^{(z)}$. In consequence, oscillations of electron density in longitudinal and vertical directions then become independent [Fig. 4(c)].

The length of the magnetic pulse has a large impact on the amplitude of oscillations of the electron's position in a nanowire. For example, for a InGaAs nanowire and $t_{\rm imp} = 20$ ps the amplitude of the expectation value of the electron's position reaches even $\bar{x}_{\rm max} = 100$ nm, while for a two times longer pulse the amplitude of electron oscillations falls to a value $\bar{x}_{\rm max} = 2.3$ nm [cf. Figs. 3(b) and 3(c)]. Despite the different lengths of these magnetic pulses, the period of oscillations in both cases is the same and equals $T_1 = 8.3$ ps, that is, the dynamics of the wave packet is governed by the energy level structure of the quantum harmonic oscillator established in the x direction. Based on the analysis of the results shown in Figs. 3(a)–3(c) and 4(a)–4(c) we may state that the time characteristics of the electron motion induced by a magnetic pulse in a bilayer nanowire strongly depends on two factors: (i) the time duration of a magnetic pulse, and (ii) the degree of asymmetry introduced to a vertical confining potential. To make it more evident we computed an expectation value of the electron's position as a function of the time duration of a magnetic pulse and the time of simulation. The results for the effective mass $m^* = 0.04$ (InGaAs) are presented in the first row in Fig. 5 for $\alpha = 0.005, 0.01, 0.02$. These α values correspond to the following energy splittings of the two lowest eigenstates for the vertical direction: $\Delta E_{21}^z = 9.9$, 10.1, and 10.9 meV. For comparison, the second row in this figure displays the results for $m^* = 0.067$ (GaAs) and energy splittings $\Delta E_{21}^z = 2.3$, 3.1, and 5.1 meV. For smaller effective mass (first row in Fig. 5) the increase of the confining potential asymmetry brings two main effects. First, the amplitude of $\bar{x}$ grows if the value of α is increased [compare the ranges of color scales in Figs. 5(a)–5(c)]. For example, for $\alpha = 0.005$ the amplitude of electron oscillations in the x direction reaches $\bar{x}_{\rm max} = 130$ nm, while for $\alpha = 0.02$ it becomes two times larger. Second, the time length of a magnetic pulse, which allows one to obtain a large amplitude of oscillations, systematically decreases for larger α values. For $\alpha = 0.005$, these oscillations disappear if the time length of the magnetic pulse equals 43.6 ps, whereas for $\alpha = 0.02$ it is limited to 17.6 ps. Oscillations still appear for longer pulses; however, they then become very weak.

For a larger effective mass (see the second row in Fig. 5 for a GaAs nanowire), the upper limit for the time length of the magnetic pulse, which may still induce a large amplitude of oscillations of the electron's position in a bilayer nanowire, is limited to less than 20 ps. In this case, however, its sensitivity to the magnitude of the potential asymmetry is not so high as for a nanowire made of InGaAs. Now, the maximal time length of a magnetic pulse decreases from 14.8 to 12.7 ps when the value of α is changed between 0.005 and 0.02. Moreover, contrary to the previous case, the largest amplitude of electron oscillations for the GaAs material becomes less dependent on the confinement asymmetry. If α's value is increased from 0.005 to 0.02, the amplitude of $\bar{x}$ does not grow much, i.e., from 210 to 250 nm. This is a three times narrower range than that predicted for a InGaAs nanowire.

B. Electron motion induced by switching the magnetic field on/off

In this section we present the results obtained for a pulse generated by switching the magnetic field on/off. The following formula describes the shape of the magnetic pulse:

$$B(t) = B_m \sin(2\pi t/t_{\rm imp} + \beta\pi/2)\Theta(t)\Theta(t_{\rm imp} - t) + \gamma B_m \Theta(t - t_{\rm imp}), \quad (8)$$

where $\beta = 0$ and $\gamma = 1$ stand for the magnetic field growing in time ($\partial B/\partial t > 0$ for $t \leqslant t_{\rm imp}$) from 0 to B_m, while $\beta = 1$ and $\gamma = 0$ for the vanishing field ($\partial B/\partial t < 0$ for $t \leqslant t_{\rm imp}$) from B_m to 0.

The results for the first case, when the magnetic field grows for $t \leqslant t_{\rm imp}$ and then it is fixed, are presented in Fig. 6. For a InGaAs wire, the dynamics of electron motion will change qualitatively and quantitatively, much as the imbalance

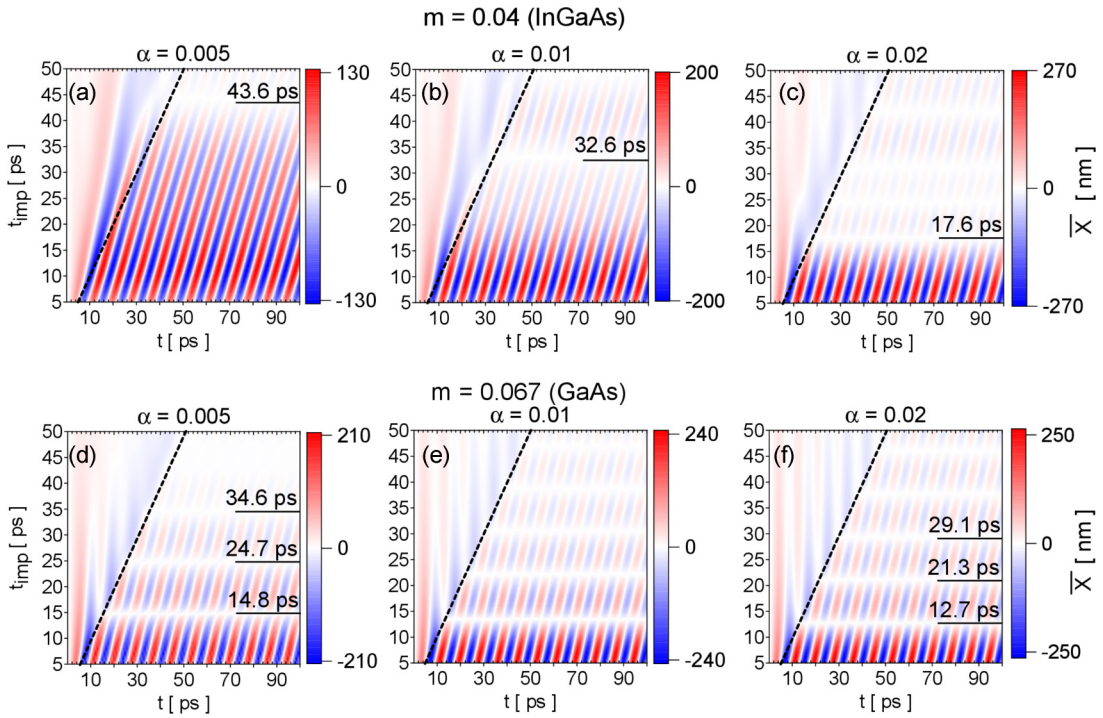

FIG. 5. Dependence of the normalized expectation value of the electron's position ($\bar{x}$) in a bilayer quantum wire on the time length of magnetic pulse and time of simulation. The inclined dashed lines mark the right border of the magnetic pulse. The upper row displays the results obtained for InGaAs, while the lower one for GaAs. The value of parameter α is shown at the top of each figure.

in the confinement energy in both layers is increased [cf. Figs. 6(a)–6(c)]. For $\alpha = 0.005$ and $\alpha = 0.01$ the pattern of $\bar{x}$ is very irregular for short pulses ($t < 10$ ps) and becomes regular, that is, with a distinct single period of oscillations for longer magnetic pulses. However, it does not concern the case with $\alpha = 0.02$ [Fig. 6(c)] for which we may single out one main period being the same for all values of t_{imp}. We will analyze the reasons for this irregularity by studying the

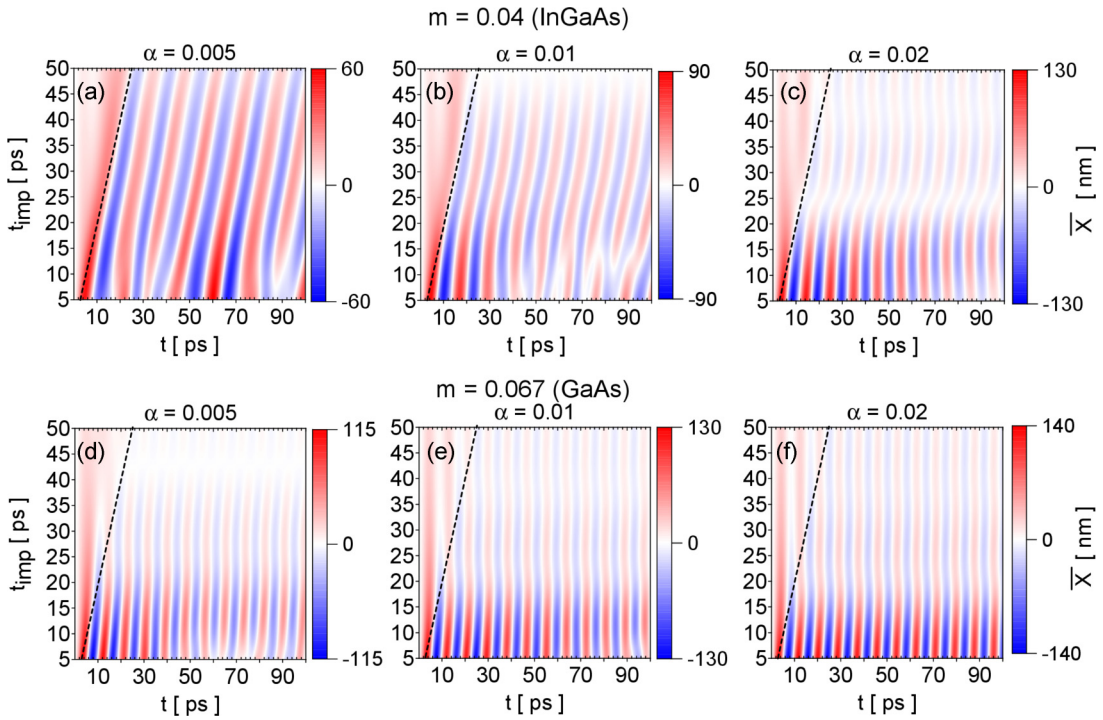

FIG. 6. Normalized expectation value of the electron's position ($\bar{x}$) in the upper layer in dependence on the time needed for switching the magnetic field on ($\partial B/\partial t > 0$ for $t < t_{\mathrm{imp}}$) and on the time of simulation. Other parameters are given at the top of the first and second rows.

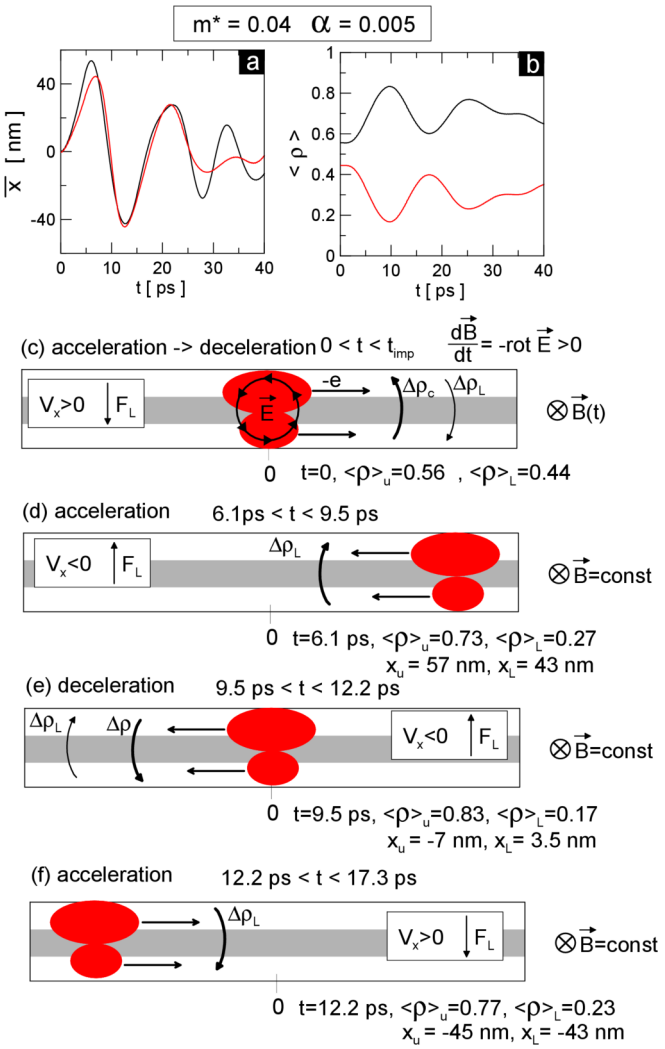

FIG. 7. Time variations of the expectation value of the electron's position (a) and of the electron density localized in the upper and lower layers (b) for increasing magnetic field and pulse length $t_{\rm imp} = 5$ ps. Black and red in (a) and (b) mark the results for the upper and lower layers, respectively. In (c)–(f) $\Delta\rho_c$ shows the direction of density flow caused by stronger localization in the upper layer, $\Delta\rho_L$ indicates the density flow forced by magnetic force, while $\Delta\rho$ marks the density flow caused by its unbalanced accumulation in layers.

changes in $\bar{x}$ and in $\langle\rho\rangle$ for both layers. These quantities, which have been calculated for parameters $t_{\rm imp} = 5$ ps, $\alpha = 0.005$, and $m^* = 0.04$, are presented in Fig. 7. In Fig. 7(a) we see that the time characteristics of $\bar{x}$ for both layers are similar for $t < 24.2$ ps, but thereafter become decoupled, even though the large amount of density may easily flow between layers, i.e., layers are still coupled [see Fig. 7(b)]. An explanation of this fact is as follows. At $t = 0$ the electron is at rest in the center of the nanowire [Fig. 7(c)] and when the magnetic field starts to grow, the rotational electric field is generated with opposite directions in the upper and lower layers. The upper layer confines a majority of the electron density which begins to move to the right according to the direction of the local electric field. Simultaneously, it pulls in this direction the remaining part of the density but against the x component of the electric field in the lower layer. Although for this right directed motion, the magnetic force is directed towards the lower layer, in fact, the density flows upwards because the growing magnetic field enhances localization of density in the deeper, upper well for $t < 5$ ps. Then the strength of the magnetic field is fixed ($B = \text{const}$) and at time instant $t = 6.1$ ps the wave packet is stopped. After that, the wave packet is turned back due to its reflection off the potential barrier on the right side [Fig. 7(d)]. In the next stage the electron moves to the left. At first, it is accelerated (6.1 ps $< t <$ 9.5 ps), and next, when it passes through the center of the nanowire ($x = 0$) it is decelerated (9.5 ps $< t <$ 12.2 ps). Since the stationary magnetic field pierces the nanosystem ($\partial B/\partial t = 0$ and $B = B_m$), the direction of magnetic force is now reversed [see Figs. 7(d) and 7(e)]. This makes an additional part of the electron density flow from the lower to the upper layer, which we have already noticed in Fig. 7(b). At time instant $t = 12.2$ ps, the decelerated electron motion is temporarily stopped on the left side of the nanowire, and next, the directions of both the wave packet and the magnetic force are again reversed. For the right directed motion, the Lorentz force now easily shifts part of the density from the upper to the lower layer. When the electron oscillates between the left and right turning points, the magnetic force makes the electron density flow between layers, which continuously perturbs and eventually hinders the upper and lower parts of the electron wave packet. Thus, an electron motion is constantly slowing down on average until the time instant $t = 24.2$ ps when the motions of the upper and lower parts of the electron wave packet eventually become decoupled and start to oscillate along the wire in an asynchronous manner [see Fig. 7(a)].

If vertical confinement becomes more asymmetric ($\alpha = 0.02$) or the effective mass is getting larger ($m^* = 0.067$), then the asynchronous motions of the upper and lower electron's densities also appear [see Figs. 8(a) and 8(c)]. In this case, however, the disproportion between the amounts of charge density localized in layers is significantly larger, e.g., we have obtained $\langle\rho\rangle_{up} = 0.7$ and $\langle\rho\rangle_{lo} = 0.3$ at $t = 0$ for $m^* = 0.04$ and $\alpha = 0.02$ [Fig. 8(b)], while for $m^* = 0.067$ the comparable fractions of density were already obtained for $\alpha = 0.005$. Such a large imbalance in density distribution for both effective masses has much less impact on the perturbation of $\bar{x}$ oscillations in the upper layer than in the lower one. The inset in Fig. 8(a) shows that the density flow between layers for the first few oscillations of $\bar{x}$ lowers only the amplitude of oscillations but motions of the upper and lower densities are still coherent. However, when the amplitude becomes smaller, e.g., for $t > 100$ ps, the electron slows down, which in consequence lowers the magnitude of magnetic force and temporarily dumps the density flow between layers [compare the amplitudes of $\langle\rho\rangle$ at the left and right sides in Fig. 8(b)]. After that, the coupling between the upper and lower densities again grows and both densities oscillate coherently. This eventually makes the amplitude of $\bar{x}$ grow. Such periodic coupling and decoupling of both densities leads to the formation of a beating pattern in $\bar{x}(t)$ if the electron oscillates in a nanowire for longer times [see Fig. 8(a)]. A similar beating pattern for $\bar{x}$ oscillations was also noticed in Fig. 8(c) for a larger effective mass, that is, for $m^* = 0.067$. In this case, even a small asymmetry in the confining potential

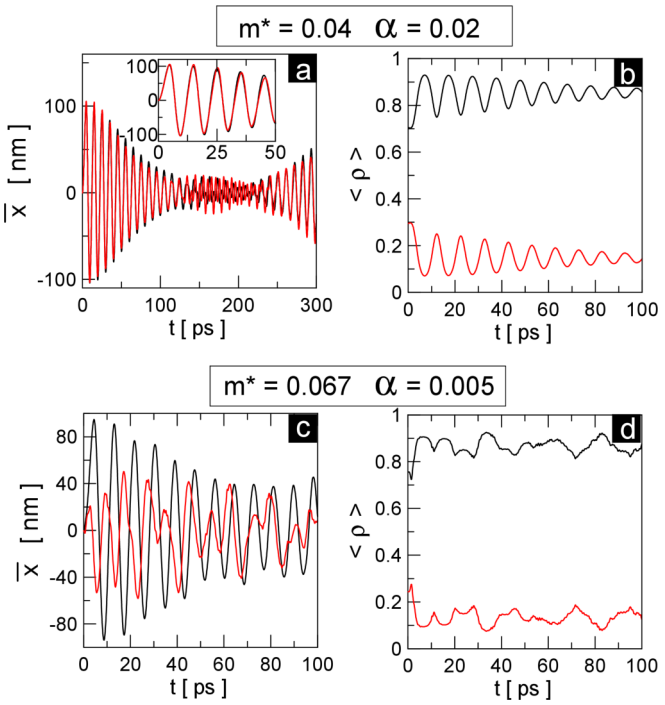

FIG. 8. Time changes of the electron's position [(a),(c)] and of densities [(b),(d)] confined in the upper and lower layers for $t_{\mathrm{imp}} = 5$ ps when the magnetic field is switching on. Black and red stand for the results obtained for the upper and for the lower layer, respectively. The values of asymmetry factor α and of effective mass are given at the top of the first and second rows.

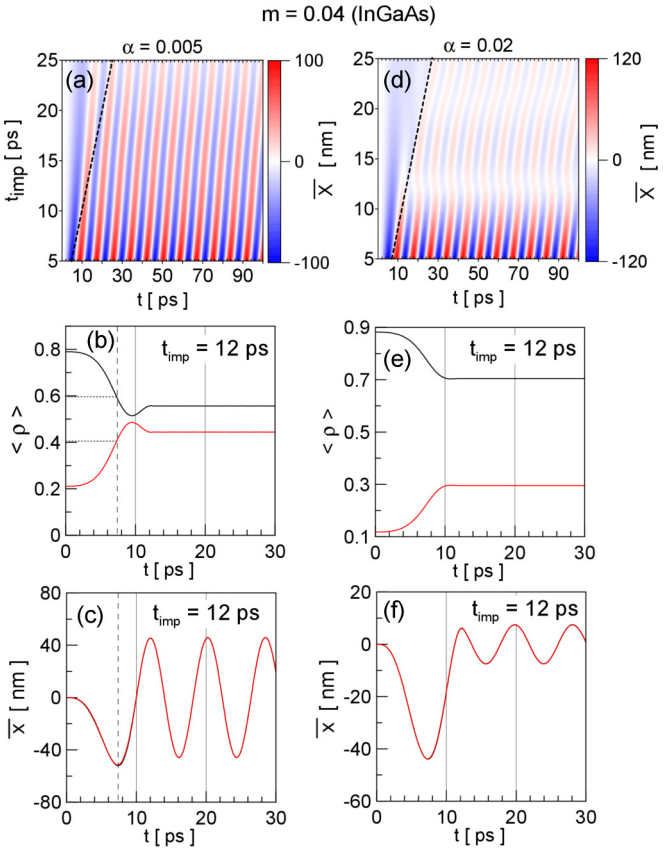

FIG. 9. (a), (d) Dependence of the electron's position $\bar{x}$ on the time duration of a magnetic pulse and on the time of simulation for the case in which the magnetic field is switched off ($\partial B/\partial t < 0$ for $t < t_{\mathrm{imp}}$ and $B = 0$ for $t > t_{\mathrm{imp}}$). (b), (e) Time variations of density confined in the upper layer (black) and in the lower layer (red). (c), (f) The normalized expectation value of the electron's position in the upper (black) and lower (red) layers (in fact, they are the same). The results in the first and second columns have been obtained for a InGaAs nanowire with asymmetry factor values set to $\alpha = 0.005$ and $\alpha = 0.02$, respectively.

($\alpha = 0.005$) is sufficient to localize about 70% of the electron density in the upper layer. Unlike the previous case, now the motions of both parts of the electron wave packet are permanently decoupled because the oscillations of density in the lower layer exhibit chaotic behavior [Fig. 8(d)]. This chaotic motion does not influence, however, the frequency of $\bar{x}$ oscillations in the upper layer, although their amplitude would be temporarily diminished.

In the last part of this section we will present the results of simulations of electron motion generated by switching the magnetic field off [$\beta = 1$ and $\gamma = 0$ in Eq. (8)]. The present case is different from that considered in Sec. III A because now the electron wave packet is prepared at $t = 0$ for $B > 0$. This means that both parts of the electron density localized in layers are already magnetically coupled at the beginning of simulation and their spatial localizations in the vertical direction become weaker when the magnetic field vanishes in time. The results for a InGaAs wire are presented in Fig. 9. Unlike the preceding case when the strength of the magnetic field was increased in time and then was fixed, now we have $B = 0$ for $t > t_{\mathrm{imp}}$ which implies that any density flow between layers must result from previous excitations of higher eigenstates in the vertical direction. Since the magnetic force is absent for $t > t_{\mathrm{imp}}$, the density localized in both layers oscillates coherently along the wire axis. Therefore, the pattern of $\bar{x}$ does not change during the simulation, i.e., the frequency of oscillations is fixed [cf. Figs. 9(a) and 9(c)]. On the other hand, an asymmetry in the confining potential again largely influences the amplitude of the electron's oscillations along the wire's axis. For a slightly asymmetric confinement ($\alpha = 0.005$), the amplitude of $\bar{x}$ in the upper layer is slowly diminished when the value of t_{imp} grows. However, if the asymmetry is increased much ($\alpha = 0.02$), the amplitude of $\bar{x}$ is suddenly reduced already for $t_{\mathrm{imp}} > 12$ ps. Such a large difference in behavior of the amplitude of oscillations obviously stems from the different dynamics of electron density in the layers for $t < t_{\mathrm{imp}}$, that is, when the layers are magnetically coupled through the nonvanishing off-diagonal elements in Hamiltonian (2). We will analyze this difference for $t_{\mathrm{imp}} = 12$ ps for which the time variations of $\langle\rho\rangle$ and $\bar{x}$ are shown in Figs. 9(b) and 9(e), and 9(c) and 9(f), respectively. In Fig. 9(b) we notice that for $\alpha = 0.005$ about 80% of the electron density is localized in the upper layer for $t = 0$. When the magnetic field is getting smaller, the electric field generated in a bilayer wire pushes the upper, major part of the density to the left, which drags the lower one in this direction too. Both densities then move coherently [see Fig. 9(c)]. However, since the magnetic field now fades out, the vertical localization of the density in each layer can no longer be as strong as it was at

the beginning of the simulation. For this reason, the electron density starts to flow from the upper to the lower layer. This process is additionally enhanced by the magnetic force which is directed downwards. At time instant $t = 7.4$ ps, when the upper and lower densities are turned back in the barrier region [minimum of $\bar{x}$ in Fig. 9(c)], 20% of the total density has been transferred to the lower layer. After reversing the direction of the electron's velocity, the lower part of the wave packet is now accelerated by an electric field while the upper part is decelerated by it. This makes the density continue to flow from the upper to the lower layer until it becomes almost equally distributed, i.e., $\langle\rho\rangle_u = 0.51$ and $\langle\rho\rangle_l = 0.49$ for $t = 9.5$ ps [see Fig. 9(b)]. This takes place just before the electron will pass the center of the wire [cf. Figs. 9(b) and 9(c) for $t = 0$]. In the next 2 ps, the direction of the density flow is again reversed and when the magnetic field is finally turned off, about 56% of the total density is localized in the upper layer while 44% is in the lower one.

If distortion in the vertical confinement is larger ($\alpha = 0.02$), even 90% of the total density can be confined in the upper layer at $t = 0$ [Fig. 9(e)] but then it falls to 78% when it reaches the turning point on the left side. When the wave packet's velocity is reversed, the larger part of the density is strongly decelerated by an electric field which in effect significantly diminishes the amplitude of oscillations of the electron's position in the x direction [Fig. 9(f)]. Therefore, we may conclude that for the longer time intervals needed for switching the magnetic field off, the dynamics of the majority of the electron density for $\alpha = 0.02$ might not adapt to the time scale of the magnetic pulse, which in consequence would prevent the electron from gaining the large values of $\bar{x}$ [see Fig. 9(d) for $t_{\rm imp} > 12$ ps].

C. Magnetically driven charge flow in nanosystems including one and two quantum wells

We have utilized the effect of magnetic stimulation of electron motion in simulations of charge transfer between two quantum wells as well as between a quantum well and two external reservoirs of electrons. In calculations, the full-period magnetic pulse was used, which has been defined in Eq. (4).

In the first case, we model the confining potential with a smooth double-hat potential

$$V(x) = V_l \exp\left[-\frac{(x-x_l)^2}{\sigma_l^2}\right] + V_r \exp\left[-\frac{(x-x_r)^2}{\sigma_r^2}\right] + xeF, \tag{9}$$

where $V_{l\ (r)}$, $x_{l\ (r)}$, and $\sigma_{l\ (r)}$ are the depths, positions of centers, and widths of the left and the right well, respectively, while F is an intensity of electric field which shifts energy levels in both wells. In calculations we have used the following values for these parameters: $V_l = V_r = -1$ meV, $x_l = 250$ nm, $x_r = 550$ nm, and $\sigma_1 = \sigma_2 = 50$ nm. Simulations were performed for a GaAs nanowire and asymmetry factor $\alpha = 0.02$.

The double-well potential is shown in Fig. 10(a). The electric field generated by external gates shifts upwards the energy levels in the right well with respect to those in the left one. For this reason, the electron wave function is initially ($t = 0$) confined in the left well. When a magnetic pulse pierces the system, the basis states $\{f_k\}$ are hybridized forcing

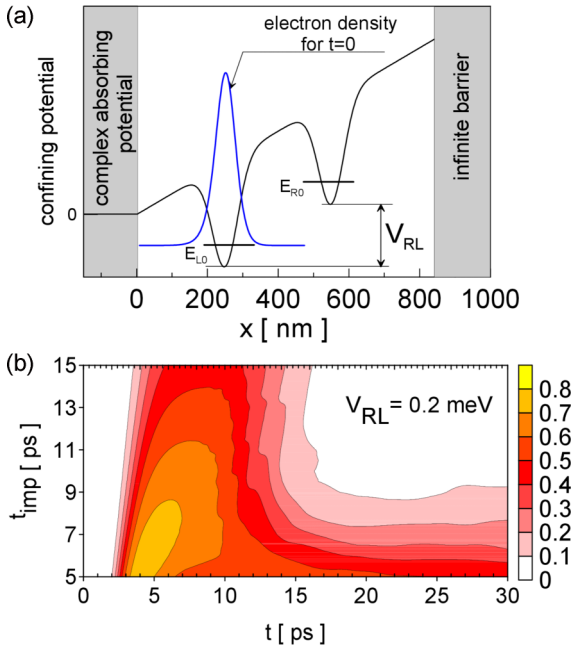

FIG. 10. (a) Double-well potential (black) with initially one electron localized in the left, lower well (blue). V_{rl} stands for the energy shift between the bottoms of two wells. (b) The time changes of electron density in the upper well region in dependence on the time duration of a magnetic pulse and for $V_{rl} = 0.2$ meV.

the electron motion to the right against the local direction of electric field. We estimate the amount of charge transferred to the upper well by integrating in time the probability current density in the middle of the distance between the wells. For the x component of the probability current density we have used the following expression which takes into account an averaging over the z variable:

$$j_x(x,t) = \sum_{k=1}^{M}\sum_{m=1}^{M}\left[-\frac{i\hbar}{2m^*}\delta_{k,m}\left(\psi_k^*(x,t)\frac{\partial\psi_m(x,t)}{\partial x} - \psi_m(x,t)\frac{\partial\psi_k^*(x,t)}{\partial x}\right) + \omega_c(t)Z_{k,m}^{(1)}\psi_k^*(x,t)\psi_m(x,t)\right]. \tag{10}$$

On the right side of the considered nanosystem we have imposed an infinite barrier, while on the left we have placed a sink that absorbs an electron wave packet. The reflectionless boundary condition on the left side prevents the electron from returning to the upper well, which may introduce some ambiguities in the results of simulations.

Figure 10(b) shows the time variations of charge which have passed through the middle of the system. The time duration of the magnetic pulse was changed between 5 and 15 ps and the energy levels shift was set to $V_{rl} = 0.2$ meV. In first few picoseconds of simulation the dynamics of electron motion is very fast and the amount of charge that has been shifted to the right region fluctuates between 0.4 and 0.8e. This value strongly depends on the time duration of the magnetic pulse. Generally, the upper limit is reached provided that the time

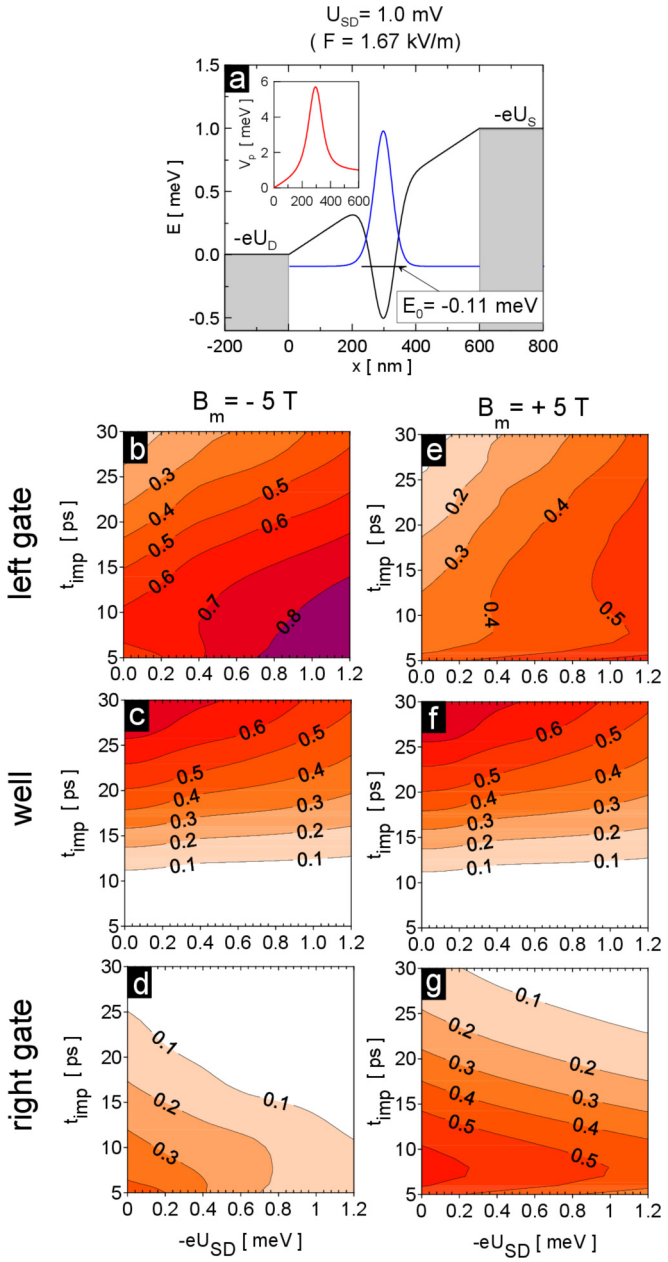

FIG. 11. (a) Single electron density (blue) confined in a quantum well (black) that is placed between two gates (gray). The inset shows the contribution to the confining potential originated from the charge density localized in the well. (b)–(d) and (e)–(g) show the fractions of single electron density confined in the left gate [(b),(e)], in the well [(c),(f)] and in the right gate [(d),(g)] depending on the time duration of the magnetic pulse (t_{imp}) and the bias voltage (U_{SD}) for the antiparallel ($B_m = -5$ T, left column) and the parallel ($B_m = +5$ T, right column) direction of the temporary magnetic field.

duration of the magnetic pulse is less than 8 ps. However, after the pulse is finished, a large fraction of the electron charge, which has a too large kinetic energy to be confined in the right well, immediately comes back to the left region. Only an application of short pulses with $t_{\mathrm{imp}} < 9$ ps guarantees that the upper well may permanently confine a significant part, i.e., more than half of the single electron charge.

In the second example, an electron is initially confined in a single quantum well [we set $V_r = 0$ in Eq. (9)] which is placed between two external gates, source and drain, respectively. The shape of the confining potential is shown in Fig. 11(a). Since the energy of the electron which has been confined in the well is less than the electrochemical potentials in both gates, it prefers to stay in the well, provided that, condition $\partial_t B = 0$ is fulfilled. The charge localized in the center of the system creates a barrier potential which is felt by other carriers gathered in the reservoirs and thus prevents the current from flowing through the well. In this configuration, the considered system fully utilizes the Coulomb blockade effect. If a magnetic pulse pierces the nanosystem, it increases the value of the electron's kinetic energy. This, in turn, forces its motion in a particular direction which depends strictly on whether the temporary magnetic field is antiparallel or parallel to the y-axis direction. In the first case, for $\vec{B} = (0,-|B(t)|,0)$ the electron is pushed to the left by the time-varying electric field where it is further accelerated due to the nonzero slope of the confining potential. It finally escapes to the left reservoir [Fig. 11(a)]. Because the left-directed electron motion temporarily strongly screens the left gate, the well shall then be filled by an electron coming from the right gate and the resulting direction of current flow would agree with the bias voltage applied to the external gates. This mechanism shall be very effective if the time length of the magnetic pulse is less than 10 ps. Then, the larger part of the electron density is easily transferred to the left reservoir [Fig. 11(b)], the central quantum well becomes temporarily empty [see Fig. 11(c)], while the remaining, minor fraction of density, of which the amount depends on the bias voltage, goes to the right reservoir [Fig. 11(d)].

In the second case, the direction of the magnetic field is reversed and the electron initially confined in the well is pushed to the right where the barrier height grows [Fig. 11(a)]. Figure 11(g) shows that the fraction of electron density shifted in time interval $t \in [0,t_{\mathrm{imp}}]$ to the right reservoir, where it is absorbed, reaches moderate values, i.e., >50% only for short pulses ($t_{\mathrm{imp}} = 7 - 10$ ps), provided that the bias voltage does not exceed 1 mV. If the electron is transferred to the right reservoir, it temporarily screens the right gate which shall allow one of the electrons from the left reservoir to enter the well. This means that for at least 50% of the total number of magnetic pulses, the direction of current flow would be opposite to the applied bias voltage.

Regardless of the current flow direction in both cases, the magnetic pulse is the only trigger for a current to flow. We believe that the quantum well embedded in a double-layer nanowire may serve as a building block for a magnetic valve allowing for a single electron charge transfer.

IV. CONCLUSIONS

The dynamics of a single electron's motion induced in a quantum wire by a single magnetic pulse was studied by means of computer simulations. We have shown that such motion can be realized in a semiconductor nanostructure which consists of two vertically stacked layers. If these layers are tunnel coupled, then the wave functions associated with several lowest eigenstates for the vertical direction can be easily hybridized by a magnetic field changeable in time. In such

case, the rotational electric field generated due to Faraday's law by a nonzero time derivative of $\vec{B}$ may accelerate the charge density localized in the upper and lower layers of the nanowire. For symmetric confinement in the vertical direction, the upper and lower fractions of the densities are forced to move always in opposite directions according to the local directions of the electric field. However, it was proven that the electron wave packet, as a whole, can be accelerated in an arbitrarily chosen direction if the confinement in layers becomes asymmetric. Then, the majority of charge density localized in one layer is pushed by the electric field and it simultaneously drags the minor part in the same direction against the electric field generated in the second layer. The dynamics of an electron wave packet becomes thus dependent on the effective mass of the electron, the degree of asymmetry in the confining potential, as well as on the time characteristics of the magnetic pulse. It was found that, generally, only the short magnetic pulses of time duration between several and maximally a few tens of picoseconds may significantly change the motion energy of the electron and its position in a nanowire. Moreover, the coherent motion of both the upper and lower parts of the wave packet can be obtained only if the magnetic coupling between layers vanishes after the magnetic pulse is finished. This takes place when a single magnetic pulse is applied to a system or the magnetic field is switched off. In the opposite case, the magnetic force constantly changes the amount of charge density confined in each layer which permanently destroys their coherent motion in a nanowire. We think that the discussed effect of magnetic stimulation of electron motion by picosecond pulses can successfully be applied in nanostructures consisting of two tunnel-coupled wires allowing one, e.g., to sample the dynamical properties of many-body interactions [15] including the Wigner crystals [16]. Moreover, this effect can also be utilized in the nanostructures holding a two-dimensional electron gas within a single, wide quantum well established in growth direction [7], allowing for studies of the dynamical properties of electron transport in quantum point contacts [17,18] or the temporary changes in the landscape of a local confining potential which is one of the essential aims of scanning (conductance) gate microscopy [17,19,20]. We have also shown that the combined effect of a Coulomb blockade and magnetic stimulation of electron motion might be utilized for the fabrication of a magnetic switch. Such switch triggered by a single magnetic pulse shall allow for single charge transfer in a bilayer nanowire even against the bias voltage applied to external gates.

ACKNOWLEDGMENTS

The work was financed by Polish Ministry of Science and Higher Education (MNiSW).

[1] C. C. Eugster and J. A. del Alamo, Phys. Rev. Lett. **67**, 3586 (1991).
[2] O. Bierwagen, C. Walther, W. T. Masselink, and K.-J. Friedland, Phys. Rev. B **67**, 195331 (2003).
[3] S. K. Lyo, J. Phys.: Condens. Matter **8**, L703 (1996).
[4] L. G. Mourokh, A. Y. Smirnov, and S. F. Fischer, Appl. Phys. Lett. **90**, 132108 (2007).
[5] S. F. Fischer, G. Apetrii, U. Kunze, D. Schuh, and G. Abstreiter, Phys. Rev. B **74**, 115324 (2006).
[6] D. Huang, S. K. Lyo, K. J. Thomas, and M. Pepper, Phys. Rev. B **77**, 085320 (2008).
[7] S. F. Fischer, G. Apetrii, U. Kunze, D. Schuh, and G. Abstreiter, Phys. Rev. B **71**, 195330 (2005).
[8] K. J. Thomas, J. T. Nicholls, M. Y. Simmons, W. R. Tribe, A. G. Davies, and M. Pepper, Phys. Rev. B **59**, 12252 (1999).
[9] J.-R. Shi and B.-Y. Gu, Phys. Rev. B **55**, 9941 (1997).
[10] T. Chwiej, Physica E **77**, 169 (2016).
[11] D. H. Auston, Appl. Phys. Lett. **26**, 101 (1975).
[12] Z. Wang, M. Pietz, J. Walowski, A. Förster, M. I. Lepsa, and M. Münzenberg, J. Appl. Phys. **103**, 123905 (2008).
[13] C. Vicario, C. Ruchert, F. Ardana-Lamas, P. M. Derlet, B. Tudu, J. Luning, and C. P. Hauri, Nat. Photonics **7**, 720 (2013).
[14] T. Chwiej, arXiv:1508.05793.
[15] S. Kumar, K. J. Thomas, L. W. Smith, M. Pepper, G. L. Creeth, I. Farrer, D. Ritchie, G. Jones, and J. Griffiths, Phys. Rev. B **90**, 201304 (2014).
[16] M. Yamamoto, H. Takagi, M. Stopa, and S. Tarucha, Phys. Rev. B **85**, 041308 (2012).
[17] S. Schnez, C. Rössler, T. Ihn, K. Ensslin, C. Reichl, and W. Wegscheider, Phys. Rev. B **84**, 195322 (2011).
[18] S. Baer, C. Rössler, E. C. de Wiljes, P.-L. Ardelt, T. Ihn, K. Ensslin, C. Reichl, and W. Wegscheider, Phys. Rev. B **89**, 085424 (2014).
[19] T. Chwiej and B. Szafran, Phys. Rev. B **87**, 085302 (2013).
[20] T. Chwiej and B. Szafran, Phys. Rev. B **89**, 195442 (2014).